Spatial heterogeneity of driving factors-induced impacts for global long-term surface urban heat island

Menglin Si, Zhao-Liang Li, Bo-Hui Tang, Xiangyang Liu, Françoise Nerry

Spatial heterogeneity of driving factors-induced impacts for global long-term surface urban heat island

Menglin Si[a,b], Zhao-Liang Li[a, b *], Bo-Hui Tang[c], Xiangyang Liu[a], and Françoise Nerry[b]

[a] *City Key Laboratory of Agricultural Remote Sensing, Ministry of Agriculture/Institute of Agricultural Resources and Regional Planning, Chinese Academy of Agricultural Sciences, Beijing 100081, China;*

[b] *ICube Laboratory, UMR 7357, CNRS-University of Strasbourg, 300 bd Sébastien Brant, CS 10413, F-67412 Illkirch Cedex, France;*

[c] *Faculty of Land Resource Engineering, Kunming University of Science and Technology, Kunming 650093, China.*

*Email: lizhaoliang@caas.cn

Spatial heterogeneity of driving factors-induced impacts for global long-term surface urban heat island

A series of empirical analytical tools have been adopted to investigate the driving mechanisms of surface urban heat islands (SUHI) on a global scale, among which spatial heterogeneity is yet to be fully elucidated. In this study, we investigated the spatial non-stationarity of the driving factors concerning surface properties, climate conditions, and urbanisation processes for global long-term SUHI. First, the potential impact on SUHI was explored using global ordinary least squares regression. Geographically weighted regression (GWR) and multi-scale GWR (MGWR) from local perspectives were employed for comparison. The results show that the MGWR has the highest goodness of fit at 0.87, 0.73, 0.90, 0.74, 0.85, and 0.76 for annual day/night (AD/AN), summer day/night (SD/SN), and winter day/night (WD/WN) scales, respectively. Although both global and local schemes exhibit similar influencing magnitudes and signs on the SUHI, the MGWR is better at capturing spatial non-stationarity. Globally, for AD, AN, SD, SN, WD, and WN, the coefficients of the urban-rural vegetation index difference (ΔEVI) and surface albedo difference (ΔWSA), urban mean precipitation (MAP), wind speed (WS), population density (PD), and urban area (UA) are -0.50, +0.30, +0.16, +1.31, -0.03, and +0.03, respectively at daytime, and -0.38, -0.33, -0.39, -0.10, +0.18, and +0.08, respectively at nighttime. Given the spatial heterogeneity of multiple factors, ΔEVI exhibits a strong mitigation effect on the SD SUHI especially in arid zones. The negative influence of ΔWSA on nighttime SUHI demonstrates a strong latitudinal disparity and greater sensitivity in the lower equatorial zone. The positive correlations between MAP and AD/SD SUHI have evident latitudinal and longitudinal variations. The mitigation effect of WS displayed distinct coastal

amplification, especially in WD. In contrast, PD and urban area UA presented prominent positive impacts on nighttime SUHI with less seasonal contrast.

Keywords: global surface urban heat island; driving factors; spatial heterogeneity; seasonal variation; day-night contrast

Introduction

With the rapid development of global economic integration and population growth, urbanisation has become a worldwide historical process (United-Nations 2019). Urban growth gradually transforms the original natural surfaces of vegetation, water, soil, and so forth into impervious urban areas that are mainly composed of built-up areas and infrastructure, accompanied by a large number of human activities (Vitousek et al. 1997). This changes the local meteorology, regional climate conditions, and energy exchange mode at the interface of the surface and the atmosphere between urban and surrounding suburban and rural areas (Grimm et al. 2008; Oke 1982). Consequently, urban or metropolitan regions become hotter than surrounding rural areas, leading to the surface urban heat island (SUHI) phenomenon (Oke 1988; Weng, Lu, and Schubring 2004). The advantages and disadvantages of SUHI has been proved hard to discern, though, it can reduce the consumption of energy significantly for mid-high latitude cities in winter while exhibits adverse effect to increase the frequency of heat disasters during heat waves (Bründl and Höppe 1984; Mohajerani, Bakaric, and Jeffrey-Bailey 2017). It is widely known that SUHI can negatively impacts energy use, urban population health, and air quality thus the considerable attention from scientific research teams, urban planners, and government departments (Zhao, Liu, and Zhou 2016; Santamouris et al. 2015). It is

necessary to enhance the theoretical research on drivers for global SUHI to support effective mitigation strategies in urban management (Zhou et al. 2019).

As a vital phenomenon reflecting the urban thermal environment, SUHI is the consequence of the combined effects of surface properties, human activities, and meteorological and climate conditions (Li, Si, and Leng 2020). Urbanisation is the primary cause of alterations in surface attributes. Modifications in the LULC and surface structure constantly alter the surface physical properties and lead to differences in the surface energy redistribution modes between urban and rural areas, which further determines the spatiotemporal pattern of the SUHI (Mika et al. 2018; Feranec et al. 2019; Lee et al. 2011; Zhao et al. 2014). Human activities have dramatically increased energy consumption and generated a large amount of waste heat, leading to additional surface heat flux, which affects the urban climate and near-surface temperature (Jin et al. 2019; Meng and Dou 2016; Yan et al. 2016). Background meteorology and climate conditions, such as differences in surface turbulence, precipitation, air temperature, wind, and cloud conditions, over urban and suburban areas often vary across different geographical regions or background climate zones (Zhao et al. 2014; Zhao 2018; Manoli et al. 2019; Sun et al. 2019; Li, Zha, and Wang 2020), which also has a strong impact on the SUHI. Although the driving factors for the characteristics of SUHIs have been thoroughly explored for several decades (He 2018; Deilami, Kamruzzaman, and Liu 2018; Zhou et al. 2019), many inconsistencies exist in the current findings owing to different time ranges, regional scopes, and analysis methods (Clinton and Gong 2013; Zhou, Rybski, and Kropp 2017; Zhou et al. 2014). Globally, there has been minimal investigations on the disparity in response mechanisms for SUHI over different regions and at different temporal scales out of annual-summer-winter and day-night aspects. Therefore, revealing

the spatial heterogeneity of the driving factors of global SUHI from a local perspective is necessary and beneficial in the proposal of targeted mitigation guidance.

To investigate the causality of SUHI, model-based schemes and statistical methods are used universally in the analytical aspect of the driving factors. Based on the surface energy balance (SEB), the underlying mechanisms of SUHI can be scientifically and physically determined (Zhao et al. 2014; Li et al. 2019). However, either the model simulation or the numerical deduction process is time-consuming and difficult to conduct on a global scale. Therefore, statistical models are more commonly used in SUHI studies (Li, Si, and Leng 2020), wherein a series of analysis tools have been adopted, such as correlation analysis (Zhou et al. 2016; Weng 2001; Tran et al. 2006), linear regression models (Dissanayake et al. 2019), spatial association analysis (Chen, Jiang, and Xiang 2016), and geographically weighted regressions (Buyantuyev and Wu 2010; Deilami and Kamruzzaman 2017). However, spatial heterogeneities of relationships generally exist between global SUHI and associated influencing factors, which are hardly detected by traditional statistical methods (Chakraborty and Lee 2019; Chakraborty et al. 2020; Peng et al. 2012). Few studies have focused on the global heterogeneity of impacts on SUHI, the driving mechanisms of global SUHI from global to local perspectives still require further investigation. Advanced spatial statistical models such as the commonly used geographically weighted regression (GWR) are recommended to better reveal the spatial heterogeneity of the driving factors for global SUHI (Li, Zha, and Zhang 2020b), however, due to the limitation of fixed bandwidth of the GWR model, improved analytical tools should be introduced to better quantify the global variation of multiple drivers for SUHI.

To this end, this study aims to explore the potential driving factors of the dynamic surface properties (surface vegetation condition and albedo), climatic conditions

(precipitation and wind), and urbanisation processes (population and urban size) for the spatial variation of global long-term SUHI with an improved spatial statistical model. The two analytical perspectives of global and local aspects were considered simultaneously as a primitive attempt to reveal the driving mechanisms of SUHI. Meanwhile, the spatial heterogeneity of the driving factors for global daytime/nighttime SUHIs on the annual, summer, and winter average scales were also disclosed by an advanced spatial statistical model.

Data

The land surface temperature was extracted from the LST products (MOD11A1 and MOD11A1, Version 6) onboard the Terra and Aqua satellites, either of which is a daily surface temperature/emissivity product dataset with a spatial resolution of 1 km. Annual land cover types were extracted from the MODIS land cover product (MCD12Q1, Version 6). The Enhanced Vegetation Index (EVI) was extracted from the vegetation index product (MOD13A2 and MYD13A2, Version 6) onboard the Terra and Aqua satellites, with a spatial resolution of 1 km. Surface albedo was extracted from the MCD43A3 (version 6) dataset. Daily images were generated using 16 days of data (centred on a given date) with a spatial resolution of 500 m. The white-sky albedo (WSA) was selected in this study as it is linearly related to black-sky albedo and demonstrates a similar impact on SUHI (Peng et al. 2012). The surface elevation was extracted from the GTOPO30 dataset, with a spatial resolution of 1 km, from the US Geological Survey. The meteorological elements were extracted from the monthly climate and climatic water balance datasets for global terrestrial surfaces - TerraClimate with a spatial resolution of 2.5 arc minutes (~ 5 km). Monthly averaged precipitation and wind speed datasets were

selected for this study. The population density in the years 2000, 2005, 2010, 2015, and 2020 was obtained from the Gridded Population of the World (GPW, v4.11) population grid density estimation data with a spatial resolution of 30 arc seconds (~ 1 km). For all available datasets, the time span was from January 2003 to December 2019, and the spatial resolution was resampled to 1 km with a sinusoidal projection. For years with missing data between 2003 and 2019, the annual global population density was constructed by borrowing the dataset of its neighbouring years.

Methodology

Definition of SUHII

The instantaneous SUHI intensity (SUHII) was defined as the LST difference between the urban and rural regions as in Equation (1).

$$SUHII_t = T_{t\_urban} - T_{t\_rural} \quad (1)$$

where the subscript t represents the four time points when Terra transitions at 10:30 and 22:30 and Aqua transitions at 13:30 and 01:30, respectively. T_{t_urban} and T_{t_rural} were the mean LSTs for urban and rural regions, respectively. Subsequently, the SUHIIs from the MOD and MYD were averaged to obtain the daily mean daytime and nighttime SUHIIs. Surface elevation data were used to filter the rural pixels which had an elevation difference of more than 50 m from the mean urban elevation. Urban and rural boundaries were defined by a dynamic urban-extent method, where the urban regions were identified by city cluster algorithms with yearly land cover data, and the rural boundaries are defined as the equal-areal buffers after excluding water and impervious surfaces (Peng et al. 2012; Si et al. 2022). Finally, the SUHII at the annual, summer, and winter scales was averaged from daily quantification. The summer months of summer (June, July, and August) and winter (December, January, and February) for the Northern Hemisphere are opposite to

that for the Southern Hemisphere.

Driving factor indices

Compared with the natural surface in rural areas, the surface energy sources in urban areas have extra radiation from anthropogenic heat, in addition to solar radiation and atmospheric downward radiation. The energy received by the earth's surface is used for heat exchange between the earth and atmosphere in the form of turbulent flow, as well as for soil heat exchange. Taking rural LST as a reference, changes in the net surface short-wave radiation will cause changes in the emission of surface long-wave radiation, which in turn will cause the redistribution of surface energy. The LST change in urban areas can be deduced by a combination of the urban-rural difference of each term related to Equation (1) (Lee et al. 2011). Correspondingly, the difference in surface radiation input and energy distribution directly leads to LST differences between urban and rural areas, that is, the SUHI phenomenon. However, as surface energy flux data with high spatial and temporal resolution and accuracy are difficult to retrieve, several proxy indicators are commonly used to reflect energy variance. Generally, changes in urban atmospheric conditions, surface properties, and climate factors cause differences in net surface shortwave net radiation and surface downward longwave radiation between urban and rural regions.

Based on the findings of previous studies (Li, Si, and Leng 2020; Sun et al. 2016; Yang, Huang, and Tang 2019; Sun et al. 2019; Manoli et al. 2019), several potential factors associated with surface properties, background climate conditions, and urbanisation were selected to analyse the driving mechanisms of global SUHII at multiple temporal scales. The surface EVI and WSA differences between the urban and rural regions (ΔEVI, ΔWSA) were calculated using the same method as that in Equation (1). The monthly accumulated precipitation (MAP) and wind speed (WS) in the urban region

were averaged to represent the climatic conditions. As for the factors related to urbanisation, the mean urban population density (PD) was assumed to be invariant within a year, and the PD for the years lacking the GPWv411 data was derived from the nearest year, while the urban area (UA) was calculated according to the previously recognised urban clusters. Thereafter, ΔEVI, ΔWSA, MAP, WS, PD, and UA were averaged at annual, summer, and winter scales.

Analytical method

From a global perspective, multiple regression analysis was used to analyse the driving factors of SUHI across cities on annual, summer, and winter averaged scales. In a traditional global regression model, ordinary least squares (OLS) methods are typically used, thus the OLS regression was used by a step-wise process to obtain the influencing factors of multiple drivers at global scale. The long-term average SUHII and each indicator were averaged by time and the regression were conducted by annual, summer, and winter scales, respectively.

Spatial regression models

Considering the spatial variability of the driving mechanism for SUHI from a local perspective, the relationship between SUHI and the related driving factors in different regions also varies with geographical location, which is called spatial non-stationarity. An advanced spatial statistical model can fully consider the first law of geography and detect the non-stationarity of the spatial relationship between variables. Therefore, GWR and multi-scale geographically weighted regression (MGWR) models were simultaneously introduced to further explore the driving factors of global SUHI at multiple spatial and temporal scales.

GWR is a modelling method for local relationships that helps explain spatial relationships under spatial heterogeneity or spatial non-stationary conditions

(Fotheringham, Brunsdon, and Charlton 2003). In contrast to OLS, which can only estimate coefficients in the global sense, GWR uses the local weighted least-squares method to estimate point-by-point parameters by incorporating the spatial position of the observation into the equation. The weight is a function of the distance between the regression point and other observation points, resulting in a continuous and smooth parameter estimation surface (Brunsdon, Fotheringham, and Charlton 1996). The GWR model extends the traditional global regression model and adds geographic location parameters, as follows:

$$y_j = \beta_0\left(u_j, v_j\right) + \sum_{i=1}^{p} \beta_i\left(u_j, v_j\right) x_{ij} + \varepsilon_j \tag{2}$$

where, $\left(u_j, v_j\right)$ is the coordinate representing the position, $\beta_0\left(u_j, v_j\right)$ is the intercept at position j, $\beta_i\left(u_j, v_j\right)$ is the local estimation parameter of the independent variable x_{ij}, p is the number of variables, ε_j is the residual at position j. Considering distance attenuation, the GWR model executes the modification by weighting the observations around all sample points. Commonly used weight matrix models include the distance threshold, k-neighbour, quadratic kernel function, and Gaussian kernel function matrices. The most frequently used Gaussian kernel function is chosen as the weight function which embodies the bandwidth for controlling the local regression.

Previous studies have proven that GWR is not sensitive to the choice of weight function, but is very sensitive to the bandwidth of the weight function. In view of the heterogeneous distribution of global SUHI and its drivers, the adaptive variable bandwidth was employed in this study, and the corrected Akaike Information Criterion (AIC_c) was introduced to determine the optimal model (Fotheringham, Brunsdon, and Charlton 2003). To evaluate the credibility of the model, it was necessary to further calculate the spatial autocorrelation coefficient of the residuals. The global Moran's I

index with a value range of [-1,1] was selected. A negative value indicates a negative spatial correlation, that is, high and low values will accumulate in a cluster; a positive value indicates a positive spatial correlation, that is, a cluster of high and high values, or low and low values, will accumulate in a cluster. A higher absolute value of the spatial autocorrelation coefficient indicates stronger spatial autocorrelation (Moran 1950).

With respect to the fact that the GWR model has a scale effect, that is, the effects of certain variables may vary on different scales, while others at the same location may be spatially stable (Goodchild 2001). Accordingly, Fotheringham et al. (2017) proposed the MGWR model whose essence was designed by relaxing the assumption that all the spatially varying processes in a model operate at the same spatial scale. An optimal bandwidth vector takes place for each particular geographical process considering in reality the discrepancy occurs between micro- and macroprocesses or between local and global processes (McMaster and Sheppard 2004). Specifically, the spatial scale at which the conditional relationship between the dependent and each predictor was confirmed to produce a more powerful spatial model MGWR. The mathematical theory behind is to replace the fixed bandwidths in GWR as flexible for each independent variable indicating different processes as follows:

$$y_j = \beta_0\left(u_j, v_j\right) + \sum_{i=1}^{p} \beta_{bwi}\left(u_j, v_j\right) x_{ij} + \varepsilon_j \tag{3}$$

where the subscript bwi in β_{bwi} indicates the bandwidth used for calibration of the ith conditional relationship.

Whereas the GWR model constrain the local relationships within each model to vary at the same spatial scale, MGWR allows the conditional relationships between the response variable and the different predictor variables to vary at different spatial scales, which is closer to the real-world geographic processes (Yang 2014). Therefore, the MGWR model was introduced to compare with the GWR model which were exploited

within the MGWR software (Oshan et al. 2019) to analyse the spatial non-stationarity of the driving factors for SUHII, and the results were compared with the findings from traditional multivariate regression schemes.

Results

Model diagnosis

Collinearity analysis

In statistical models, the linear correlation between two or more predictors is called multicollinearity (Alin 2010). Due to the non-independence of predictor variables, multiple variables may synchronously explain a certain underlying mechanism, resulting in larger deviations in model parameter estimates. In order to avoid the influence of multicollinearity, the Variance Inflation Factor (VIF) is usually used to judge whether multicollinearity exists between the selected predictor variables before the regression analysis. Generally, the closer the VIF is to 1, the smaller the collinearity (Dormann et al. 2013). The VIF of the aforementioned six driving factors (ΔEVI, ΔWSA, MAP, WS, PD, and UA) are listed in Table 1. Because there is no day-night variation in the selected variable, the day-night VIF is equal. The VIF value of each variable was close to 1 and far below the threshold value of 10. Therefore, it can be considered that there is no prominent multicollinearity between the selected factors, which can be used for the subsequent analysis of the multiple regression model.

Table 1 Variance inflation factor (VIF) of explanatory variables

	ΔEVI	ΔWSA	MAP	WS	PD	UA
Annual daytime	1.38	1.25	1.47	1.24	1.10	1.04
Annual nighttime	1.38	1.25	1.47	1.24	1.10	1.04
Summer daytime	1.11	1.22	1.30	1.29	1.06	1.03
Summer nighttime	1.11	1.22	1.30	1.29	1.06	1.03

Winter daytime	1.39	1.21	1.22	1.16	1.12	1.05
Winter nighttime	1.39	1.21	1.22	1.16	1.12	1.05

Diagnostic Information

The model fitting and diagnosis information for the multivariate regression, GWR, and MGWRs models at the average annual, summer, and winter scales are shown in Table 2. The diagnosis results of the OLS, GWR, and MGWR models change with day-night and seasonal variations. For each temporal scale, the AICs values of the OLS, GWR, and MGWR models gradually decreased, and the lower AICs of GWR and MGWR models indicate a reduction of model complexity which can better avoid the model overfitting than that of OLS. The coefficients of determination (R^2) of the OLS regression models are 0.57, 0.24, 0.67, 0.24, 0.34, and 0.31, respectively, which are worse than those of the GWR and MGWR models for the different temporal scales. The R^2 values of the MGWR model are 0.87, 0.73, 0.90, 0.74, 0.85, and 0.76, respectively. Moreover, compared with the OLS model, the absolute values of Moran's I for the GWR and MGWR models are closer to 0, indicating that they can effectively capture the spatial non-stationarity of the driving factors, and that MGWR performs better than GWR. In general, the explanatory factors of the SUHII have spatial non-stationarity, and the MGWR model has the optimal performance for the interpretation of global SUHI from a local perspective.

Table 2 Diagnostic Information of OLS, GWR and MGWR models

	Annual daytime	Annual nighttime	Summer daytime	Summer nighttime	Winter daytime	Winter nighttime
OLS diagnostics						
AICs	3407.272	4398.981	2975.548	4401.896	4170.915	4235.052
R^2	0.575	0.240	0.670	0.237	0.335	0.310
R^2 adjusted	0.573	0.238	0.669	0.234	0.333	0.307
Moran's Index	0.521	0.440	0.668	0.451	0.572	0.489
GWR diagnostics						
AICs	2029.597	3415.593	1697.603	3264.442	2404.918	3147.025

R^2	0.867	0.731	0.889	0.760	0.856	0.757
R^2 adjusted	0.843	0.668	0.869	0.700	0.820	0.707
Moran's Index	0.033	0.074	0.045	0.038	0.033	0.059
MGWR diagnostics						
AICs	1926.200	3258.350	1613.605	3237.352	2276.312	3057.863
R^2	0.871	0.733	0.897	0.743	0.846	0.759
R^2 adjusted	0.850	0.682	0.878	0.689	0.818	0.714
Moran's Index	-0.032	-0.001	0.006	0.004	-0.012	-0.003

Model comparison for regression coefficients

Table 3 shows a comparison of the regression coefficients of the OLS, GWR, and MGWR methods. The regression coefficients of the OLS model are unique on a global scale. For the GWR and MGWR models, the global average and variance of the local coefficients are provided. The OLS model has an insignificant parameter fitting at a 95% confidence interval on several scales. Given the results of the three models, the regression coefficients of ΔEVI are all negative, the regression coefficients of ΔWSA and MAP are positive during the day and negative at night, and the regression coefficients of WS are all negative, while the regression coefficients of PD and UA are positive in most cases. The sign of the influence of each factor on the SUHII is consistent with the results of previous studies, while the magnitudes vary between different models due to different fitting process, which indicates the reasonability and reliability of the regression models for characterising the drivers for SUHII (Si et al. 2022; Peng et al. 2012; Chakraborty and Lee 2019) .

Table 3 Regression coefficients of OLS, GWR and MGWR models

	Annual daytime	Annual nighttime	Summer daytime	Summer nighttime	Winter daytime	Winter nighttime
OLS global regression						
Intercept	-0.000	-0.000	0.000	0.000	0.000	0.000
ΔEVI	-0.544	-0.182	-0.719	-0.216	-0.469	-0.111
ΔWSA	0.152	-0.184	0.241	-0.068	-0.024*	-0.392
MAP	0.243	-0.452	0.047	-0.427	0.211	-0.297
WS	-0.037	-0.264	-0.076	-0.012*	-0.141	-0.259
PD	-0.065	0.147	-0.058	0.106	-0.028*	0.125
UA	0.152	0.026*	0.143	0.085	0.107	0.001*
GWR local regression (mean ± std)						
Intercept	0.032 ± 0.548	0.000 ± 0.781	0.104 ± 0.533	-0.877 ± 4.485	-0.071 ± 0.711	-0.264 ± 1.042
ΔEVI	-0.500 ± 0.256	-0.302 ± 0.372	-0.584 ± 0.241	-0.335 ± 0.314	-0.356 ± 0.432	-0.130 ± 0.380
ΔWSA	0.305 ± 0.218	-0.300 ± 0.316	0.313 ± 0.166	-0.127 ± 0.251	0.391 ± 0.459	-0.412 ± 0.434
MAP	0.201 ± 0.240	-0.429 ± 0.611	0.132 ± 0.397	-1.140 ± 4.118	0.199 ± 0.842	-0.860 ± 1.597
WS	-0.106 ± 0.190	-0.079 ± 0.346	-0.077 ± 0.167	-0.090 ± 0.315	-0.074 ± 0.274	-0.058 ± 0.377
PD	0.030 ± 0.339	0.151 ± 0.383	0.021 ± 0.214	0.108 ± 0.255	0.053 ± 0.279	0.204 ± 0.332
UA	-0.009 ± 0.235	0.237 ± 0.559	0.008 ± 0.218	0.193 ± 0.405	-0.057 ± 0.348	0.211 ± 0.514
MGWR local regression (mean ± std)						
Intercept	-0.081 ± 0.363	-0.037 ± 0.589	0.127 ± 0.399	-0.725 ± 1.078	-0.189 ± 0.408	-0.130 ± 0.302
ΔEVI	-0.497 ± 0.232	-0.380 ± 0.290	-0.589 ± 0.248	-0.341 ± 0.197	-0.362 ± 0.359	-0.160 ± 0.245
ΔWSA	0.302 ± 0.186	-0.331 ± 0.314	0.286 ± 0.147	-0.146 ± 0.204	0.419 ± 0.429	-0.425 ± 0.291
MAP	0.156 ± 0.025	-0.394 ± 0.440	0.147 ± 0.247	-1.086 ± 1.493	0.177 ± 0.218	-0.632 ± 0.647
WS	-0.131 ± 0.195	-0.100 ± 0.116	-0.075 ± 0.110	-0.165 ± 0.174	-0.095 ± 0.030	-0.056 ± 0.275
PD	-0.030 ± 0.124	0.177 ± 0.163	-0.003 ± 0.132	0.122 ± 0.062	-0.036 ± 0.136	0.216 ± 0.204
UA	0.031 ± 0.017	0.080 ± 0.137	0.019 ± 0.114	0.136 ± 0.345	-0.020 ± 0.236	0.067 ± 0.150

(*Insignificant, p>0.05)

Spatial non-stationarity

Figure 1–Figure 6 show the spatial distribution of the regression coefficients of each

driving factor obtained from the MGWR model, corresponding to the daytime and nighttime conditions in annual, summer, and winter scales. The colour symbols represent different coefficient intervals, whereas the grey circles represent points where the estimation is insignificant ($p>0.05$). It is clear that the regression coefficients for each driving factor show a large spatial variance.

For the annual daytime SUHII in Figure 1, ΔEVI has a significant negative contribution in most cities around the world, indicating that the increase in vegetation activity means a greater daytime evapotranspiration, which leads to a decrease in SUHII. In arid regions, such as North Africa and the Middle East, where cities with cold islands are distributed (Si et al. 2022), the negative contribution of ΔEVI is more evident. There is a positive correlation between ΔWSA and annual daytime SUHII, and the coefficients vary across different latitude zones. The MAP is positively correlated with the annual daytime SUHII for most cities, and South America displays the largest coefficient magnitude. The WS shows a significant negative contribution in some cities. PD has the largest positive correlation in cities on the east coast of Australia, followed by cities in Southeast Asia and northeastern China. Significant negative correlations appear in some cities in North America, Western Europe, and Africa. UA has significant positive correlations mainly in North America, South America, Africa, and Western Europe in the Western Hemisphere, where PD shows a large proportion of negative contributions.

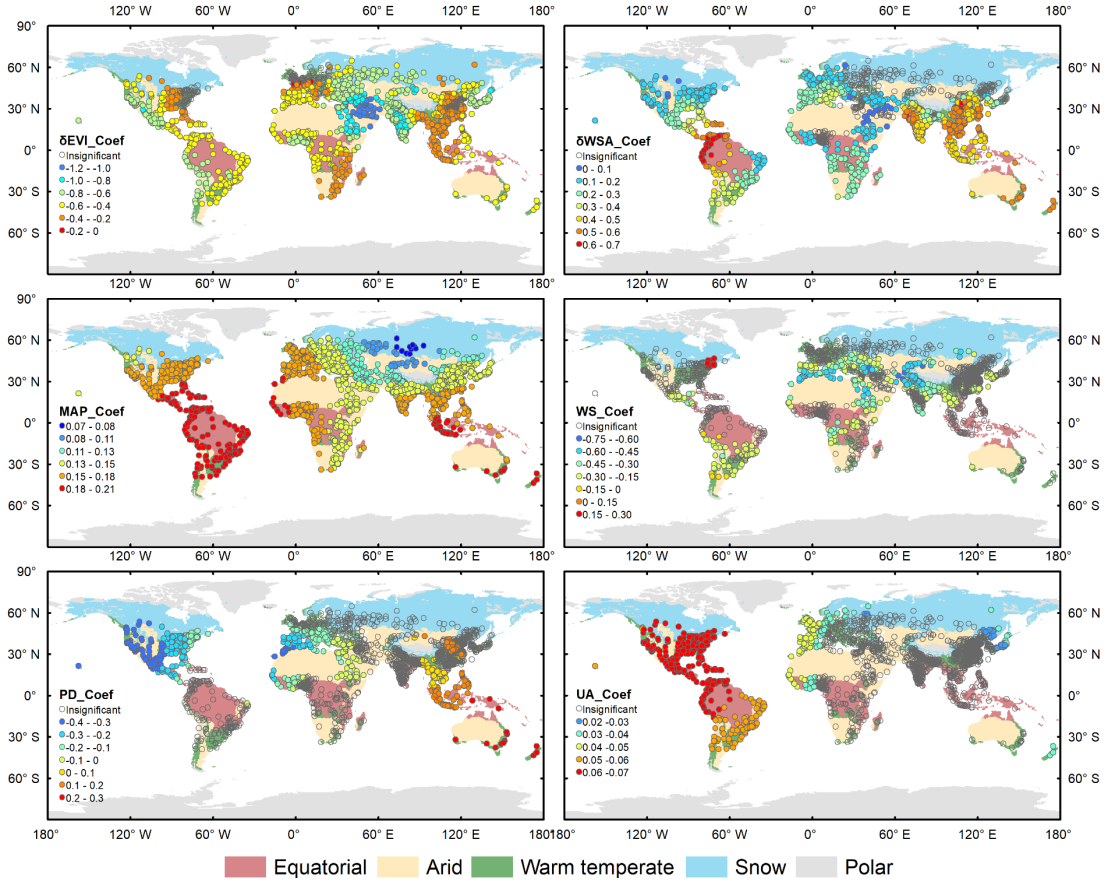

Figure 1 The spatial variation of coefficients of multi-independents for annual daytime SUHII.

According to Figure 2, for the annual nighttime SUHII, the correlation of ΔEVI in most cities is significantly reduced. ΔWSA has a negative correlation with the annual nighttime SUHII, whose magnitude gradually decreases from the equatorial region to high latitudes, and a few positive contributions arise in the Southern Hemisphere. According to Equation (4), ΔWSA and solar radiation regulate nighttime SUHII by influencing the net surface shortwave radiation during the daytime. Normally, the intensity of solar radiation in the equatorial region is higher than that at high latitudes; thus, equatorial SUHII is more sensitive to changes in ΔWSA. MAP is negatively correlated with annual nighttime SUHII, while the number of cities with a significant correlation decreased compared with daytime cases. WS shows negative correlations, while the absolute value of the coefficients is lower than that during the daytime. It is inferred that the WS has a smaller impact on the impedance at night, which leads to a

weaker regulation effect on the sensible heat flux than during the day. For PD in developed countries such as the United States, Europe, and other regions, the positive correlation at night is greater than in developing countries, while it is relatively minimal in India. The positive effect of UA in North America and South America is weaker at night than during the day, whereas the impact on the SUHII in the Middle East and India has increased significantly, which may be related to the emission of more heat fluxes from human activities in these areas.

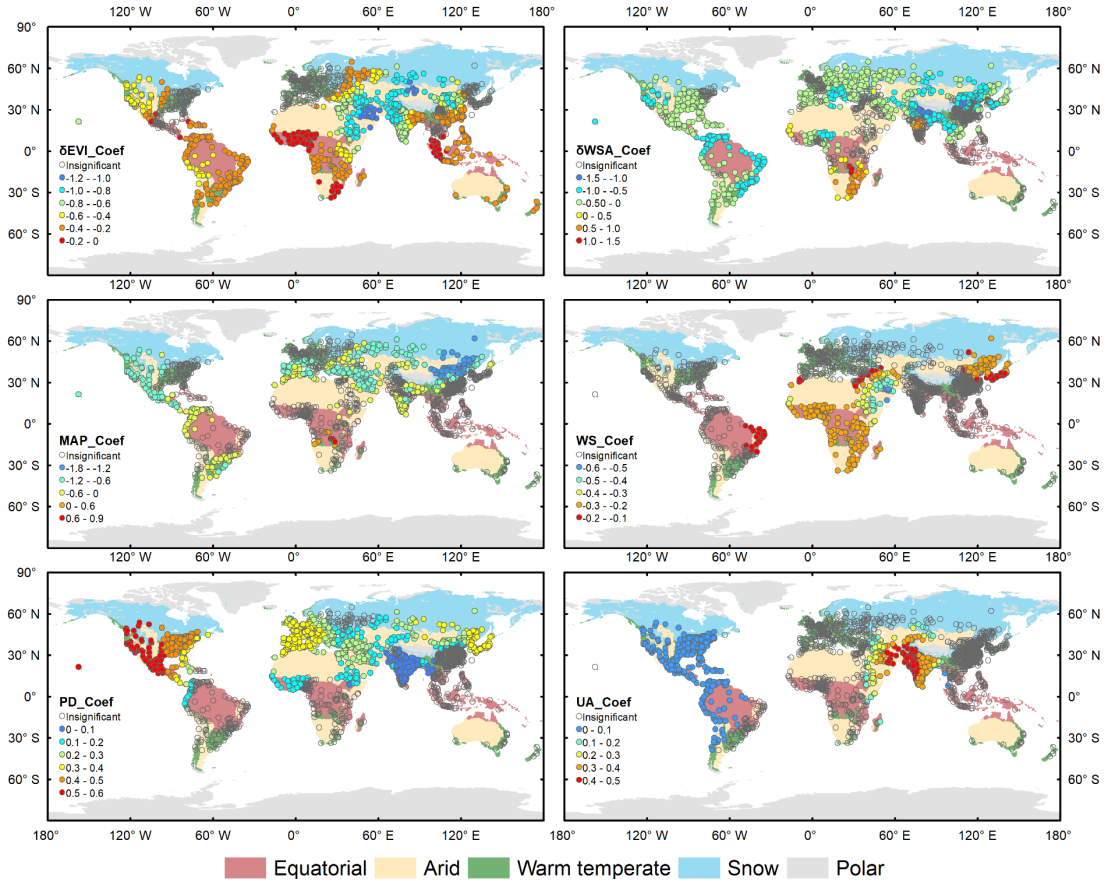

Figure 2 The spatial variation of coefficients of multi-independents for annual nighttime SUHII.

Figure 3 and Figure 4 show the spatial distribution of the regression coefficients of the summer daytime and nighttime SUHII, respectively. The negative correlation of ΔEVI with summer daytime SUHII is more evident than that in the annual cases. The latitudinal variations of the correlation with ΔWSA are not that obvious during the daytime, and the negative correlation at nighttime is also lower than the annual average cases. The daytime

positive correlation and nighttime negative correlation with MAP in the Northern Hemisphere are significantly higher than those in the Southern Hemisphere. This may be related to the stronger vegetation activities in the Northern Hemisphere during summer. Precipitation not only regulates the evaporation ratio by affecting the surface soil moisture but also promotes the growth of vegetation, making summer SUHII in the Northern Hemisphere more sensitive to changes in MAP. The negative influence of WS on summer SUHII at night is stronger than that during the daytime. PD had a significantly higher impact on SUHII at night than during the day. UA is significantly positively correlated with summer daytime SUHII in North America and Western Europe in the Western Hemisphere, while in India, the impact of UA is stronger on nighttime SUHII.

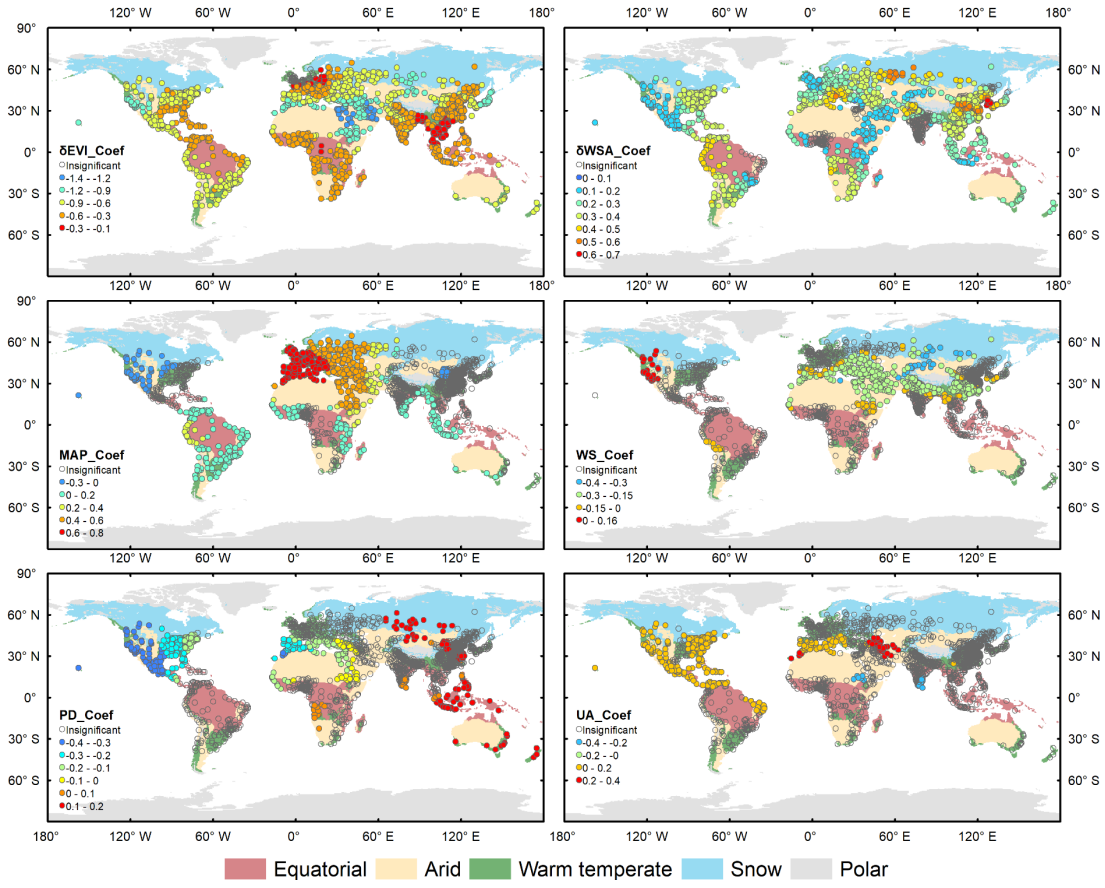

Figure 3 The spatial variation of coefficients of multi-independents for summer daytime SUHII.

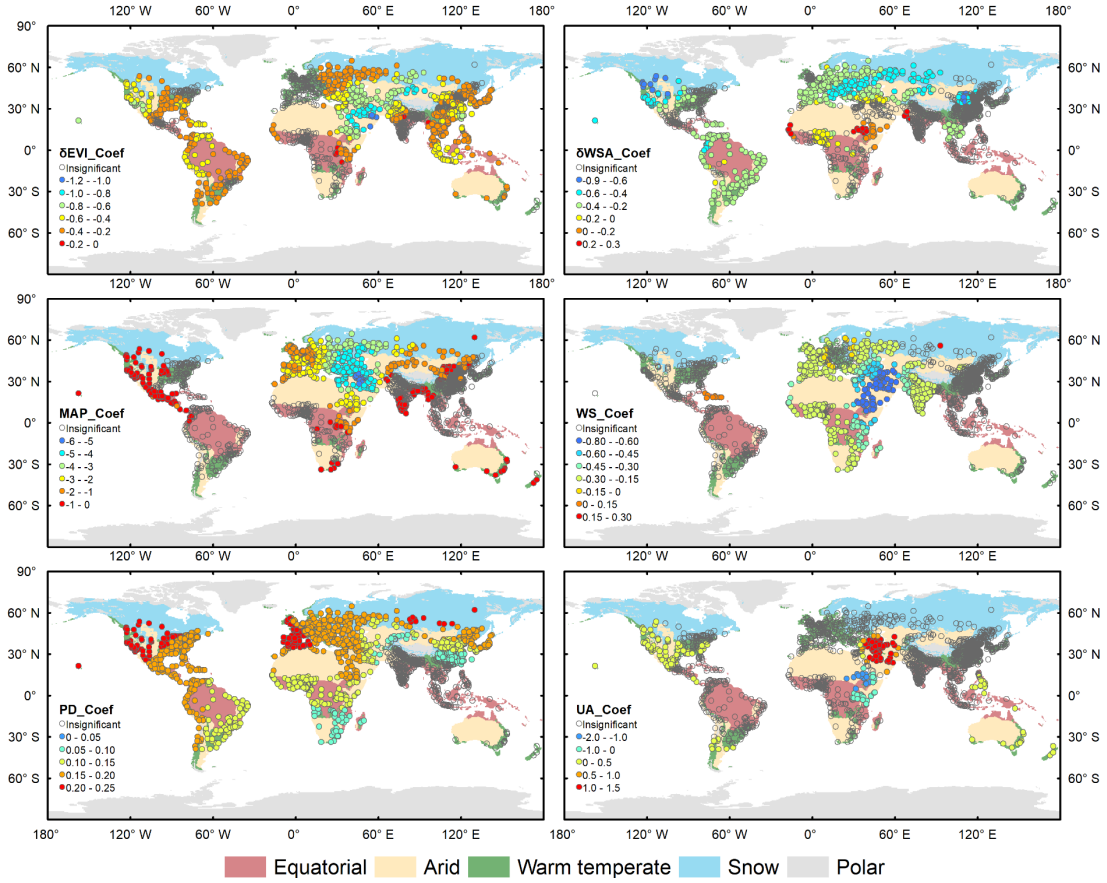

Figure 4 The spatial variation of coefficients of multi-independents for summer nighttime SUHII.

Figure 5 and Figure 6 show the spatial distribution of the regression coefficients of the winter daytime and nighttime SUHII, respectively. Compared with the results in summer, the negative contribution of ΔEVI in the daytime is relatively weaker, which may be related to the weakening of vegetation activities in winter. The positive correlation of ΔWSA with winter SUHII shows limited significance during the daytime, while the negative correlation at nighttime shows a decreasing magnitude from the equator to higher latitudes. In winter, the positive correlation between MAP and daytime SUHII is more obvious in the equator and arid zone, while the magnitude of the negative correlation between MAP and nighttime SUHII decreases from the equator to the poles. WS shows a negative correlation, which is more evident during the daytime than at nighttime. PD and UA had significant positive contributions, especially at night. In most cities in the Northern Hemisphere, PD is more positively correlated with nighttime SUHII.

The positive contribution of UA at night is greater in areas such as East Africa and India.

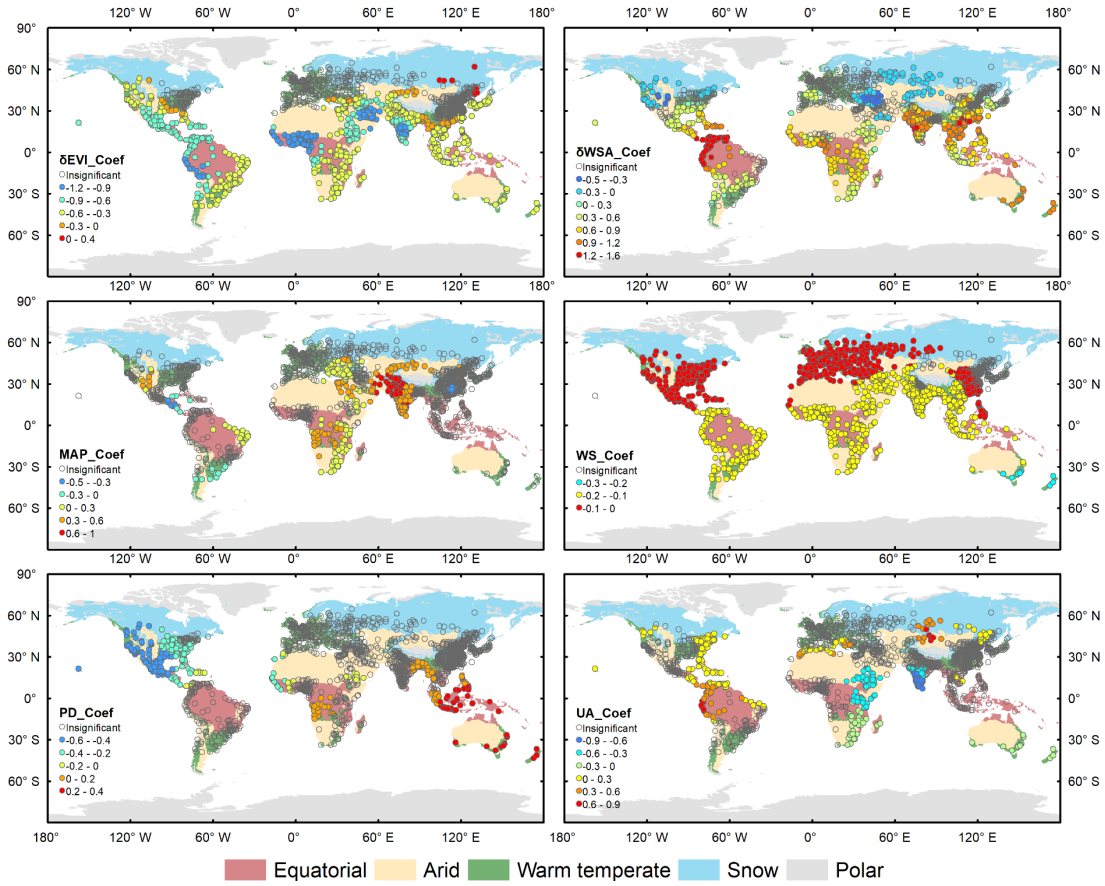

Figure 5 The spatial variation of coefficients of multi-independents for winter daytime SUHII.

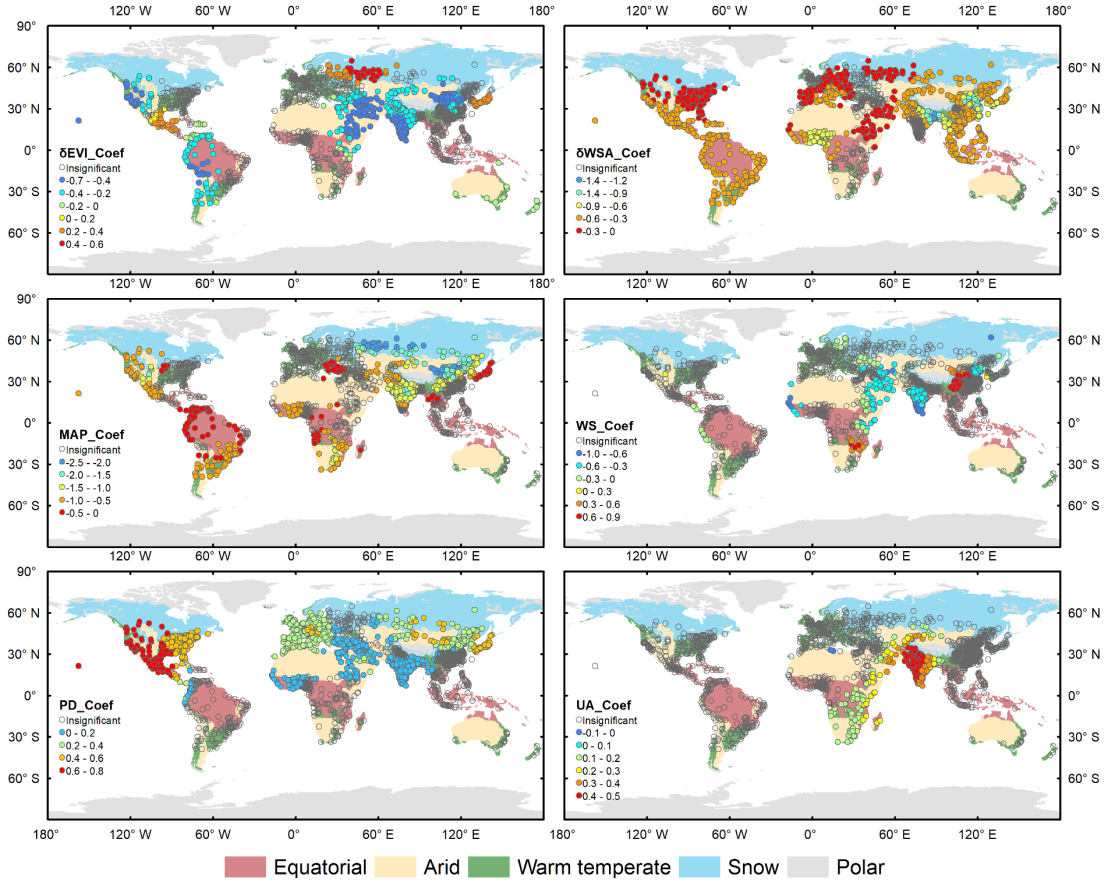

Figure 6 The spatial variation of coefficients of multi-independents for winter nighttime SUHII.

Discussion

As one of the most severe urban thermal environmental problems, the SUHI phenomenon based on remote sensing technology acts as a bridge between research on satellite product algorithms and urban remote sensing applications. In view of the uncertainty of the driving mechanisms and the deficiency of heterogeneity of the influencing effect for global long-term SUHI, this study proposes the necessity of exploring the spatial and temporal variation of influencing magnitude and signs by introducing advanced spatial statistical models. First, the global daily instantaneous daytime and nighttime SUHII dataset from 2003 to 2019 were generated and averaged over different seasons. Second, the driving factors for the global SUHII were analysed from a global perspective, which was further compared with the GWR and MGWR models at the local scale. The results

and findings are expected to provide target indications for mitigation policies in urban management in different geographic regions.

Impact of multiple factors

Based on the regression from the three schemes, the results prove that the average contributions of the different statistical models show consistent evidence. Generally, ΔEVI is negatively correlated with daytime SUHII, which is mainly caused by the effect of vegetation activity on the latent heat flux. ΔWSA mainly regulates nighttime SUHII by affecting the net surface shortwave radiation during the day and surface heat storage at night. The MAP was positively correlated with daytime SUHII and negatively correlated with nighttime SUHII, which mainly affects the specific heat capacity, surface impedance, and other parameters related to the surface heat flux in rural natural land surface, resulting in different rates of LST increase during the day and LST decrease at night to regulate the daytime and nighttime SUHII. WS mainly contributes negatively to SUHII by disturbing the surface impedance and regulating the sensible heat flux. The positive correlation between PD and UA with SUHII was more significant at nighttime, mainly due to anthropogenic heat emissions amplifying SUHII.

Although we have compared three different analytical methods, the execution of each model was simultaneously used one by one in order to keep the consistency for impact analysis on global cities. Previously, most SUHI studies have focused on a single city or representative cities and urban clusters on a national or regional scale (Sun, Wang, and Wang 2020; Li, Zha, and Zhang 2020a; Hu et al. 2019; Yue et al. 2019; Sun et al. 2019; Lai et al. 2021), whereas the impact analysis on long-term SUHI at a global scale has been less conducted (Wu and Ren 2019). Specifically, the relationship between spatially distributed SUHII and associated drivers may not necessarily be consistent due to the different definition of urban and rural regions, various analytical approach, and

even different data source (Li et al. 2023). For example, studies at the global scale show that city size has a positive impact on SUHI (Zhou, Rybski, and Kropp 2017), while studies at the regional scale showed no significant correlation between them (Zhou et al. 2014). To avoid this inconsistency as much as possible, this work presented a comprehensive study across global cities with long-term time span and based on identical analysis method.

Spatial non-stationarity

The limited global studies (Zhang et al. 2010; Peng et al. 2012; Clinton and Gong 2013) did not completely analyze the spatial variation of impacts on SUHI. In this study, we revealed the spatial heterogeneity of multiple factor-induced impact on global long-term SUHI. Under the combined effect of multiple factors, the driving mechanism of the global SUHII is spatially nonstationary for different seasons. During the day, larger differences in vegetation activity between urban and rural areas generally produce a stronger intensity of cold islands in arid regions, where the evaporative heat flux dominates more significantly and shows a larger negative coefficient on ΔEVI. At night, the influence of ΔEVI was weak across the globe. The contribution of ΔEVI is mainly from the summer scale.

As for ΔWSA, the insignificant positive correlations with daytime SUHII were not apparent globally. The negative magnitude of its coefficient at night has a latitudinal effect, indicating global solar radiation distribution. The magnitude of the contribution is larger in equatorial regions, where higher solar radiation exists and decreases at higher latitudes. Generally, the ΔWSA in winter shows a more obvious negative contribution than in summer, and the nighttime SUHII is dominated by the negative effect of ΔWSA in the higher latitudinal zone where snow cover appears more frequently.

The positive correlations between the daytime SUHII and MAP showed latitudinal and longitudinal variations. At the annual scale, there is a trend of decreasing correlations from low latitudes to high latitudes and from the Western to Eastern hemisphere. The highest contributions were distributed in the equatorial regions of South America. At night, the negative contribution of MAP also shows a larger magnitude in the Northern Hemisphere, with a limited number of significant correlations compared to daytime conditions. Specifically, in summer, the disparity between the Northern and Southern Hemispheres is obvious both during the day and night. In the Northern Hemisphere with higher vegetation activity, the LST is more sensitive to surface soil moisture and vegetation growth, thus has a larger contribution to SUHII from MAP. In winter, the influence of MAP is weak compared with in summer.

As for WS, its negative contribution in some cities also displays spatial variability, and the magnitude of the effect is relatively larger in coastal cities. Regarding the summer-winter contrast, the WS in winter daytime shows significant and larger cooling effects on SUHI in most cities across the globe. At night, the WS shows negative correlations, while the absolute value of the coefficients is lower than that of during the day. It is inferred that the WS has a smaller impact on the impedance at night, which leads to a weaker regulation effect on the sensible heat flux at night than during the day.

PD showed significant positive correlations with daytime SUHII in cities in the Eastern hemisphere, while negative correlations appeared in regions with larger positive UA contributions, mainly distributed in some Western cities. At night, the sign and magnitude of PD are even larger in Western developed countries, where the positive contribution of UA becomes weaker, which shows contrary regulation as that at daytime. There was no significant summer-winter difference in the influencing effect of PD and UA on its spatial heterogeneity.

Implications and prospects

The driving factors for SUHI have been fully investigated for several decades; however, SUHI is typically quantified using land surface temperature, which is a spatial variable at the local scale. Assessing the spatial heterogeneity of the driving mechanisms for global long-term SUHI at multiple temporal scales is usually not a point of focus. In this study, we presented a comprehensive investigation on the influencing effects of multiple factors on global SUHI from global to local perspective and distinguished the day-night and summer-winter contrast with an improved MGWR model. To the best of our knowledge, this work has been paid little intention in previous global SUHI studies. This proves to be a significant consideration in further detection of global SUHI and its underlying mechanisms. Meanwhile, our findings exhibit magnitudes and signs of drivers consistent with the results from a global perspective in previous studies, indicating that different quantification schemes of driving mechanism assessment may not affect the average pattern of influencing factors for global SUHI. The findings on global SUHI variation and its associated factors are assumed to have implications for urban planning. Furthermore, it is necessary to assess additional potential driving factors of anthropogenic activities (e.g. air pollution and human heat flux) and urban landscapes (Cao et al. 2016; Li et al. 2018; Liu and Weng 2009; Lu and Weng 2006; Weng and Lu 2008; Huang and Wang 2019).

Generally, spatial non-stationarity is assessed using advanced spatial statistical models, which can also be applied to SUHI research. To further reveal the temporal heterogeneity of global long-term SUHI, we analysed the disparity of spatial non-stationarities of driving factors by distinguished temporal scales, that is, day-night and summer-winter contrast. With the development of more advanced simultaneous

spatiotemporal GWR models in the future, the findings of this study are expected to be further validated using other schemes.

Conclusions

Revealing the driving mechanisms for the global SUHI effect, especially at multiple spatial and temporal scales, is essential in the provision of more targeted mitigation policies for improving the urban thermal environment. This study explored the driving factors and spatial non-stationarity of the global long-term SUHI at multiple temporal scales. Based on the previously proposed dynamic urban-extent method, the daily instantaneous daytime and nighttime SUHII was quantified for global cities from 2003 to 2019. The driving indices concerning the surface properties, climate conditions, and urbanisation process were constructed by referring to the SEB model. By employing multilinear regression, the influencing magnitude and sign of multiple drivers for SUHI were preliminarily uncovered from a global perspective. From a local perspective, to further recover the driving mechanisms and spatial heterogeneity of multiple factors, the advanced spatial statistical models GWR and MGWR were introduced and compared with the OLS method. The model comparison showed that advanced GWR and MGWR schemes exhibited a better model fitting effect, and the latter performed best and uncovered the spatial heterogeneity of driving factors for global SUHI. Finally, the spatial non-stationarity of each factor, that is, the global pattern of the coefficients for annual, summer, and winter SUHIIs, at daytime and nighttime, respectively, was further revealed by the MGWR model.

This study mainly draws the following findings:

(1) The results from the MGWR model provide an optimal estimation of the contribution coefficients compared to the GWR and OLS models. For MGWR diagnosis, the R^2 values were the highest (0.87, 0.73, 0.90, 0.74, 0.85, and 0.76), and the absolute

values of Moran's I were closest to 0 for different temporal scales. The contribution of multiple factors to global SUHI is spatially non-stationary.

(2) ΔEVI was negatively correlated with daytime SUHII, which is more sensitive in arid regions. The summer-winter contrast of its influence is evident.

(3) The day-night difference for ΔWSA mainly comes from the insignificant positive and significant negative coefficients of the daytime and nighttime SUHIIs, respectively. The latitudinal variation in the negative contribution of ΔWSA is more obvious in winter and more sensitive to larger solar radiation in the lower latitudinal zone compared with in summer.

(4) Evident latitudinal and longitudinal variation appears in the positive correlations between MAP and annual and summer daytime SUHII, which decreases from lower to higher latitude zones and from the Western to Eastern Hemisphere. At night, the negative contribution of MAP is superior in the Northern Hemisphere, but with limited significant cases.

(5) The WS is mainly a negative contribution to daytime and nighttime SUHII, which shows a more evident effect along coastal cities and a significant summer-winter contrast with a larger contribution during winter daytime.

(6) The positive correlations between PD and UA with SUHII are more significant at night, with less seasonal contrast. The day-night disparity mainly originates from the daytime negative correlations from PD, accompanied by a larger positive UA contribution in some Western cities, and vice versa at nighttime.

Acknowledgements

We would like to acknowledge the Google Earth Engine platform for providing MODIS, Terra Climate, and topographic data, and the cloud computing capability free of charge. This work was supported by the National Natural Science Foundation of China (Grant

No. 41921001 and No. 42201404), and the China Postdoctoral Science Foundation (No. 2022M723439). The author Menglin Si would like to thank the China Scholarship Council for the financially support of her stay in ICube, France.

Reference

Alin, Aylin. 2010. "Multicollinearity." *Wiley Interdisciplinary Reviews: Computational Statistics* 2 (3):370-4.

Bründl, W., and P. Höppe. 1984. "Advantages and disadvantages of the urban heat island —an evaluation according to the hygro-thennic Effects." *Archives for meteorology, geophysics, and bioclimatology, Series B* 35 (1):55-66. doi: 10.1007/BF02269409.

Brunsdon, C., A. S. Fotheringham, and M. E. Charlton. 1996. "Geographically weighted regression: A method for exploring spatial nonstationarity." *Geographical Analysis* 28 (4):281-98. doi: 10.1111/j.1538-4632.1996.tb00936.x.

Buyantuyev, A., and J. G. Wu. 2010. "Urban heat islands and landscape heterogeneity: linking spatiotemporal variations in surface temperatures to land-cover and socioeconomic patterns." *Landscape Ecology* 25 (1):17-33. doi: 10.1007/s10980-009-9402-4.

Cao, Chang, Xuhui Lee, Shoudong Liu, Natalie Schultz, Wei Xiao, Mi Zhang, and Lei Zhao. 2016. "Urban heat islands in China enhanced by haze pollution." *Nature Communications* 7:1-7. doi: 10.1038/ncomms12509.

Chakraborty, T, A Hsu, D Manya, and G Sheriff. 2020. "A spatially explicit surface urban heat island database for the United States: Characterization, uncertainties, and possible applications." *ISPRS Journal of Photogrammetry and Remote Sensing* 168:74-88.

Chakraborty, T, and X Lee. 2019. "A simplified urban-extent algorithm to characterize surface urban heat islands on a global scale and examine vegetation control on their spatiotemporal variability." *International Journal of Applied Earth Observation and Geoinformation* 74:269-80.

Chen, Liang, Rong Jiang, and Wei Ning Xiang. 2016. "Surface heat island in Shanghai and its relationship with urban development from 1989 to 2013." *Advances in Meteorology*. doi: 10.1155/2016/9782686.

Clinton, Nicholas, and Peng Gong. 2013. "MODIS detected surface urban heat islands and sinks: Global locations and controls." *Remote Sensing of Environment* 134:294-304. doi: 10.1016/j.rse.2013.03.008.

Deilami, K., and M. Kamruzzaman. 2017. "Modelling the urban heat island effect of smart growth policy scenarios in Brisbane." *Land Use Policy* 64:38-55. doi: 10.1016/j.landusepol.2017.02.027.

Deilami, Kaveh, Md Kamruzzaman, and Yan Liu. 2018. "Urban heat island effect: A systematic review of spatio-temporal factors, data, methods, and mitigation measures." *International Journal of Applied Earth Observation and Geoinformation* 67 (January):30-42. doi: 10.1016/j.jag.2017.12.009.

Dissanayake, Morimoto, Ranagalage, and Murayama. 2019. "Land-Use/Land-Cover Changes and Their Impact on Surface Urban Heat Islands: Case Study of Kandy City, Sri Lanka." *Climate* 7 (8):99-. doi: 10.3390/cli7080099.

Dormann, C. F., J. Elith, S. Bacher, C. Buchmann, G. Carl, G. Carre, J. R. G. Marquez, et al. 2013. "Collinearity: a review of methods to deal with it and a simulation

study evaluating their performance." *Ecography* 36 (1):27-46. doi: 10.1111/j.1600-0587.2012.07348.x.

Feranec, J., M. Kopecka, D. Szatmari, J. Holec, P. Stastny, R. Pazur, and H. Bobal'ova. 2019. "A review of studies involving the effect of land cover and land use on the urban heat island phenomenon, assessed by means of the MUKLIMO model." *Geografie* 124 (1):83-101.

Fotheringham, A Stewart, Chris Brunsdon, and Martin Charlton. 2003. *Geographically weighted regression: the analysis of spatially varying relationships*: John Wiley & Sons.

Fotheringham, A Stewart, Wenbai Yang, and Wei Kang. 2017. "Multiscale geographically weighted regression (MGWR)." *Annals of the American Association of Geographers* 107 (6):1247-65.

Goodchild, Michael F. 2001. "Models of scale and scales of modelling." *Modelling scale in geographical information science*:3-10.

Grimm, N. B., S. H. Faeth, N. E. Golubiewski, C. L. Redman, J. G. Wu, X. M. Bai, and J. M. Briggs. 2008. "Global change and the ecology of cities." *Science* 319 (5864):756-60. doi: 10.1126/science.1150195.

He, Bao Jie. 2018. "Potentials of meteorological characteristics and synoptic conditions to mitigate urban heat island effects." *Urban Climate* 24 (January):26-33. doi: 10.1016/j.uclim.2018.01.004.

Hu, Yonghong, Meiting Hou, Gensuo Jia, Chunlei Zhao, Xiaoju Zhen, and Yanhua Xu. 2019. "Comparison of surface and canopy urban heat islands within megacities of eastern China." *ISPRS Journal of Photogrammetry and Remote Sensing* 156 (March):160-8. doi: 10.1016/j.isprsjprs.2019.08.012.

Huang, Xin, and Ying Wang. 2019. "Investigating the effects of 3D urban morphology on the surface urban heat island effect in urban functional zones by using high-resolution remote sensing data: A case study of Wuhan, Central China." *ISPRS Journal of Photogrammetry and Remote Sensing* 152:119-31.

Jin, Kai, Fei Wang, Deliang Chen, Huanhuan Liu, Wenbin Ding, and Shangyu Shi. 2019. "A new global gridded anthropogenic heat flux dataset with high spatial resolution and long-term time series." *Scientific Data* 6 (1):139. doi: 10.1038/s41597-019-0143-1.

Lai, Jiameng, Wenfeng Zhan, Jinling Quan, Benjamin Bechtel, Kaicun Wang, Ji Zhou, Fan Huang, Tirthankar Chakraborty, Zihan Liu, and Xuhui Lee. 2021. "Statistical estimation of next-day nighttime surface urban heat islands." *ISPRS Journal of Photogrammetry and Remote Sensing* 176:182-95.

Lee, X., M. L. Goulden, D. Y. Hollinger, A. Barr, T. A. Black, G. Bohrer, R. Bracho, et al. 2011. "Observed increase in local cooling effect of deforestation at higher latitudes." *Nature* 479 (7373):384-7. doi: 10.1038/nature10588.

Li, Dan, Weilin Liao, Angela J Rigden, Xiaoping Liu, Dagang Wang, Sergey Malyshev, and Elena Shevliakova. 2019. "Urban heat island: Aerodynamics or imperviousness?" *Science Advances* 5 (4):eaau4299.

Li, Huidong, Fred Meier, Xuhui Lee, Tirthankar Chakraborty, Junfeng Liu, Martijn Schaap, and Sahar Sodoudi. 2018. "Interaction between urban heat island and urban pollution island during summer in Berlin." *Science of the Total Environment* 636:818-28. doi: 10.1016/j.scitotenv.2018.04.254.

Li, Long, Yong Zha, and Ren Wang. 2020. "Relationship of surface urban heat island with air temperature and precipitation in global large cities." *Ecological Indicators* 117:106683.

Li, Long, Yong Zha, and Jiahua Zhang. 2020a. "Spatial and dynamic perspectives on surface urban heat island and their relationships with vegetation activity in Beijing, China, based on Moderate Resolution Imaging Spectroradiometer data." *International Journal of Remote Sensing* 41 (3):882-96.

Li, Long, Yong Zha, and Jiahua Zhang. 2020b. "Spatially non-stationary effect of underlying driving factors on surface urban heat islands in global major cities." *International Journal of Applied Earth Observation and Geoinformation* 90:102131.

Li, Zhao-Liang, Menglin Si, and Pei Leng. 2020. "A review of remotely sensed surface urban heat islands from the fresh perspective of comparisons among different regions (Invited Review)." *Progress In Electromagnetics Research C* 102:31-46.

Li, Zhao-Liang, Hua Wu, Si-Bo Duan, Wei Zhao, Huazhong Ren, Xiangyang Liu, Pei Leng, Ronglin Tang, Xin Ye, and Jinshun Zhu. 2023. "Satellite remote sensing of global land surface temperature: definition, methods, products, and applications." *Reviews of Geophysics* 61 (1):e2022RG000777.

Liu, Hua, and Qihao Weng. 2009. "Scaling effect on the relationship between landscape pattern and land surface temperature." *Photogrammetric Engineering & Remote Sensing* 75 (3):291-304.

Lu, Dengsheng, and Qihao Weng. 2006. "Spectral mixture analysis of ASTER images for examining the relationship between urban thermal features and biophysical descriptors in Indianapolis, Indiana, USA." *Remote Sensing of Environment* 104 (2):157-67. doi: https://doi.org/10.1016/j.rse.2005.11.015.

Manoli, Gabriele, Simone Fatichi, Markus Schläpfer, Kailiang Yu, Thomas W. Crowther, Naika Meili, Paolo Burlando, Gabriel G. Katul, and Elie Bou-Zeid. 2019. "Magnitude of urban heat islands largely explained by climate and population." *Nature* 573 (7772):55-60. doi: 10.1038/s41586-019-1512-9.

McMaster, Robert B., and Eric Sheppard. 2004. "Introduction: Scale and Geographic Inquiry." In *Scale and Geographic Inquiry*, 1-22.

Meng, Chunlei, and Youjun Dou. 2016. "Quantifying the Anthropogenic Footprint in Eastern China." *Scientific Reports* 6.

Mika, J., P. Forgo, L. Lakatos, A. B. Olah, S. Rapi, and Z. Utasi. 2018. "Impact of 1.5 K global warming on urban air pollution and heat island with outlook on human health effects." *Current Opinion in Environmental Sustainability* 30:151-9. doi: 10.1016/j.cosust.2018.05.013.

Mohajerani, Abbas, Jason Bakaric, and Tristan Jeffrey-Bailey. 2017. "The urban heat island effect, its causes, and mitigation, with reference to the thermal properties of asphalt concrete." *Journal of Environmental Management* 197:522-38. doi: 10.1016/j.jenvman.2017.03.095.

Moran, Patrick AP. 1950. "A test for the serial independence of residuals." *Biometrika* 37 (1/2):178-81.

Oke, T. R. 1982. "The energetic basis of the urban heat island." *Quarterly Journal of the Royal Meteorological Society* 108 (455):1-24. doi: 10.1002/qj.49710845502.

Oke, T. R. 1988. "The Urban Energy Balance." *Progress in Physical Geography* 12 (4): 471–508. doi:10. 1177/030913338801200401.

Oshan, Taylor M, Ziqi Li, Wei Kang, Levi J Wolf, and A Stewart Fotheringham. 2019. "mgwr: A Python implementation of multiscale geographically weighted regression for investigating process spatial heterogeneity and scale." *Isprs International Journal of Geo-Information* 8 (6):269.

Peng, Shushi, Shilong Piao, Philippe Ciais, Pierre Friedlingstein, Catherine Ottle, François-Marie Bréon, Huijuan Nan, Liming Zhou, and Ranga B. Myneni. 2012.

"Surface Urban Heat Island Across 419 Global Big Cities." *Environmental Science & Technology* 46 (2):696-703. doi: 10.1021/es2030438.

Santamouris, M., C. Cartalis, A. Synnefa, and D. Kolokotsa. 2015. "On the impact of urban heat island and global warming on the power demand and electricity consumption of buildings—A review." *Energy and Buildings* 98:119-24. doi: https://doi.org/10.1016/j.enbuild.2014.09.052.

Si, Menglin, Zhao-Liang Li, Françoise Nerry, Bo-Hui Tang, Pei Leng, Hua Wu, Xia Zhang, and Guofei Shang. 2022. "Spatiotemporal pattern and long-term trend of global surface urban heat islands characterized by dynamic urban-extent method and MODIS data." *ISPRS Journal of Photogrammetry and Remote Sensing* 183:321-35. doi: https://doi.org/10.1016/j.isprsjprs.2021.11.017.

Sun, Ranhao, Yihe Lü, Xiaojun Yang, and Liding Chen. 2019. "Understanding the variability of urban heat islands from local background climate and urbanization." *Journal of Cleaner Production* 208:743-52. doi: 10.1016/j.jclepro.2018.10.178.

Sun, Yeran, Shaohua Wang, and Yu Wang. 2020. "Estimating local-scale urban heat island intensity using nighttime light satellite imageries." *Sustainable Cities and Society* 57:102125.

Sun, Ying, Xuebin Zhang, Guoyu Ren, Francis W. Zwiers, and Ting Hu. 2016. "Contribution of urbanization to warming in China." *Nature Climate Change* 6 (7):706-9. doi: 10.1038/nclimate2956.

Tran, Hung, Daisuke Uchihama, Shiro Ochi, and Yoshifumi Yasuoka. 2006. "Assessment with satellite data of the urban heat island effects in Asian mega cities." *International Journal of Applied Earth Observation and Geoinformation* 8 (1):34-48. doi: 10.1016/j.jag.2005.05.003.

United-Nations. 2019. "United Nations, Department of Economic Social Affairs, Population Division, 2019. World Urbanization Prospects: The 2018 Revision." In, 197-236. New York: United Nations.

Vitousek, Peter M, Harold A Mooney, Jane Lubchenco, and Jerry M Melillo. 1997. "Human domination of Earth's ecosystems." *Science* 277 (5325):494-9. doi: 10.1126/science.277.5325.494.

Weng, Q. 2001. "A remote sensing-GIS evaluation of urban expansion and its impact on surface temperature in the Zhujiang Delta, China." *International Journal of Remote Sensing* 22 (10):1999-2014. doi: Doi 10.1080/713860788.

Weng, Qihao, and Dengsheng Lu. 2008. "A sub-pixel analysis of urbanization effect on land surface temperature and its interplay with impervious surface and vegetation coverage in Indianapolis, United States." *International Journal of Applied Earth Observation and Geoinformation* 10 (1):68-83.

Weng, Qihao, Dengsheng Lu, and Jacquelyn Schubring. 2004. "Estimation of land surface temperature-vegetation abundance relationship for urban heat island studies." *Remote Sensing of Environment* 89 (4):467-83. doi: 10.1016/j.rse.2003.11.005.

Wu, Zhifeng, and Yin Ren. 2019. "A bibliometric review of past trends and future prospects in urban heat island research from 1990 to 2017." *Environmental Reviews* 27 (2):241-51. doi: 10.1139/er-2018-0029.

Yan, Zhong Wei, Jun Wang, Jiang Jiang Xia, and Jin Ming Feng. 2016. "Review of recent studies of the climatic effects of urbanization in China." *Advances in Climate Change Research* 7 (3):154-68. doi: 10.1016/j.accre.2016.09.003.

Yang, Qiquan, Xin Huang, and Qiuhong Tang. 2019. "The footprint of urban heat island effect in 302 Chinese cities: Temporal trends and associated factors." *Science of the Total Environment* 655:652-62. doi: 10.1016/j.scitotenv.2018.11.171.

Yang, Wenbai. 2014. "An extension of geographically weighted regression with flexible bandwidths." University of St Andrews.

Yue, Wenze, Xue Liu, Yuyu Zhou, and Yong Liu. 2019. "Impacts of urban configuration on urban heat island: An empirical study in China mega-cities." *Science of the Total Environment* 671:1036-46. doi: 10.1016/j.scitotenv.2019.03.421.

Zhang, Ping, Marc L. Imhoff, Robert E. Wolfe, and Lahouari Bounoua. 2010. "Characterizing urban heat islands of global settlements using MODIS and nighttime lights products." *Canadian Journal of Remote Sensing* 36 (3):185-96. doi: 10.5589/m10-039.

Zhao, Lei. 2018. "Urban growth and climate adaptation." *Nature Climate Change* 8 (12):1034-. doi: 10.1038/s41558-018-0348-x.

Zhao, Lei, Xuhui Lee, Ronald B. Smith, and Keith Oleson. 2014. "Strong contributions of local background climate to urban heat islands." *Nature* 511 (7508):216-9. doi: 10.1038/nature13462.

Zhao, Shuqing, Shuguang Liu, and Decheng Zhou. 2016. "Prevalent vegetation growth enhancement in urban environment." *Proceedings of the National Academy of Sciences* 113 (22):6313. doi: 10.1073/pnas.1602312113.

Zhou, Bin, Diego Rybski, and Jürgen P. Kropp. 2017. "The role of city size and urban form in the surface urban heat island." *Scientific Reports* 7 (1):1-9. doi: 10.1038/s41598-017-04242-2.

Zhou, Decheng, Jingfeng Xiao, Stefania Bonafoni, Christian Berger, Kaveh Deilami, Yuyu Zhou, Steve Frolking, Rui Yao, Zhi Qiao, and José A. Sobrino. 2019. "Satellite remote sensing of surface urban heat islands: Progress, challenges, and perspectives." *Remote Sensing* 11 (1):1-36. doi: 10.3390/rs11010048.

Zhou, Decheng, Liangxia Zhang, Lu Hao, Ge Sun, Yongqiang Liu, and Chao Zhu. 2016. "Spatiotemporal trends of urban heat island effect along the urban development intensity gradient in China." *Science of the Total Environment* 544 (219):617-26. doi: 10.1016/j.scitotenv.2015.11.168.

Zhou, Decheng, Shuqing Zhao, Shuguang Liu, Liangxia Zhang, and Chao Zhu. 2014. "Surface urban heat island in China's 32 major cities: Spatial patterns and drivers." *Remote Sensing of Environment* 152:51-61. doi: 10.1016/j.rse.2014.05.017.